

# Effects of various transition metals on the thermal oxidative stabilization of polyacrylonitrile nanofibers

**Jung-Hun Lee**

Sungkyunkwan University - Suwon Campus: Sungkyunkwan University - Natural Sciences Campus

**Siying Li**

Sungkyunkwan University - Suwon Campus: Sungkyunkwan University - Natural Sciences Campus

**Ji-Beom Yoo**

Sungkyunkwan University - Suwon Campus: Sungkyunkwan University - Natural Sciences Campus

**Young Jun Kim** (✉ [yjkim68@skku.edu](mailto:yjkim68@skku.edu))

Sungkyunkwan University - Suwon Campus: Sungkyunkwan University - Natural Sciences Campus

<https://orcid.org/0000-0002-9801-3066>

---

## Research Article

**Keywords:** PAN nanofibers, Transition metal, Thermal oxidative stabilization, Cyclization

**Posted Date:** February 16th, 2021

**DOI:** <https://doi.org/10.21203/rs.3.rs-230180/v1>

**License:** © ⓘ This work is licensed under a Creative Commons Attribution 4.0 International License.

[Read Full License](#)

---

**Version of Record:** A version of this preprint was published at Journal of Inorganic and Organometallic Polymers and Materials on March 15th, 2021. See the published version at <https://doi.org/10.1007/s10904-021-01954-x>.



## 1 **Introduction**

2 Polyacrylonitrile (PAN) is one of the most commonly used materials for the fabrication  
3 of carbon fibers.[1-3] To produce PAN-based carbon fibers, the polymer must first be  
4 converted to a flame-resistant structure (e.g., a ladder-like structure or a non-plastic cyclic  
5 structure) through a stabilization process[2] to prevent it from melting during carbonization.  
6 The stabilized PAN structure, which has a high rate of conversion to carbon fiber, is the  
7 reason why the PAN-based carbon fiber has outstanding properties compared with carbon  
8 fibers based on any other precursor material.[4, 5]

9 When heated from 200 °C to 300 °C in air, PAN will be transformed into a ladder-like  
10 structure through cyclization, dehydrogenation, and oxidation processes[4-6] The cyclization  
11 process converts the nitrile groups to conjugated nitrogen double bonds, which in turn forms  
12 an aromatic ring together with five carbon atoms.[7] The dehydrogenation process exhausts  
13 the hydrogen atoms by reacting with O<sub>2</sub> to form H<sub>2</sub>O. Finally, the oxidation of PAN generates  
14 oxygen-containing groups, such as carbonyl and carboxyl groups. These reactions lead to the  
15 ladder-like structure of PAN and prevent it from melting during carbonization.[8]

16 The structural conversion of PAN releases a large amount of heat, as the formation of  
17 free radicals that initiate cyclization leads to a sudden and rapid evolution of thermal  
18 energy.[7, 9, 10] Since the intense exothermic reaction can break the molecular chain of PAN,  
19 the resultant carbon fibers are left with inferior characteristics. To alleviate the intense  
20 exothermic reaction, researchers have tried to blend PAN with different co-monomers and  
21 reported the effects on the cyclization kinetics. For example, to decrease the stabilization  
22 temperature and/or alleviate the intense exothermic reaction, PAN was copolymerized with

1 itaconic acid (IA), acrylic acid (AA), an ammonium salt of itaconic acid (AIA), guanidinium  
2 itaconate (GIA), methyl acrylate (MA), methacrylic acid (MAA), or 2-acrylamido-2-  
3 methylpropane acid (AMPS).[9-18] Among these co-monomers, IA resulted in a significant  
4 decrease in the stabilization temperature and alleviated the intense exothermic reaction.[14,  
5 16-18] Unfortunately, it also decreased the cyclization rate, generating many beta-amino  
6 groups and conjugated nitrile groups, which caused point defects in the carbon fiber.[19, 20]  
7 Moskowitz et. reported GIA contained copolymers showed a significant reduction in heat  
8 flow and cyclization peak temperature as compare to IA copolymers.

9 In addition to organic materials, inorganic materials such as carbon nanotubes (CNTs)  
10 and functionalized CNTs have been mixed with the PAN precursor.[7, 21, 22] CNTs enhance  
11 the mechanical properties of the carbon fiber. Since PAN is already a one-dimensional  
12 crystallized material consisting of carbon atoms, it can easily stack upon the CNTs to form a  
13 graphitic structure. In other words, the CNTs in the PAN work as nucleation sites for  
14 graphitic structure formation.[22] However, the CNTs had a negative effect on the PAN  
15 stabilization process as the stabilization of the PAN-CNTs composite resulted in more  
16 unreacted nitrile groups than the stabilization of PAN alone. Therefore, the composite  
17 required a relatively longer stabilization time.[22]

18 Over the years, the synthesis and application of metals or metal oxides have attracted the  
19 interest of a wide range of researchers from different fields.[23-28] As another kind of  
20 inorganic additives, the study of applying transition metals and their oxides in PAN fibers by  
21 adding transition metal salts in PAN solutions for electrospinning has received much  
22 attention.[28-33] Co nanoparticles encapsulated in PAN-based carbon fibers were applied as  
23 electrocatalysts for the stable oxygen reduction reaction.[28] A core-shell structure assembled

1 by Ni(OH)<sub>2</sub> grown on NiCo<sub>2</sub>O<sub>4</sub> embedded PAN-based carbon nanofibers (CNFs) was  
2 successfully synthesized and applied as anode material in a supercapacitor.[29]  
3 Functionalized porous graphitic CNFs incorporated with iron acetylacetonate sacrificial  
4 catalyst performed exceptional rate performance in lithium-ion batteries as anode  
5 material.[30] Activated CNFs composite with Cu/Cu<sub>x</sub>O nanoparticles prepared by  
6 electrospinning of copper acetate addicted PAN solution followed by carbonization and mild  
7 activation was fabricated and its enhanced adsorption to gaseous pollutant H<sub>2</sub>S was  
8 investigated.[31] Although there are diverse studies on the applications of transition metal  
9 and metal oxide nanoparticles composite with PAN CNFs, there is a lack of studies on the  
10 reaction of metal salt additions with PAN during synthesis and subsequent stabilization.

11 Usually, transition metals can be used to reduce the activation energy of a reaction,  
12 resulting in a higher reaction rate. Therefore, in this study, we investigated the effects of  
13 several transition metals on the PAN stabilization process using differential scanning  
14 calorimetry (DSC) and Fourier-transform infrared (FTIR) spectroscopy. For this purpose, we  
15 used the acetate salts of iron (Fe), cobalt (Co), nickel (Ni), and copper (Cu). Each transition  
16 metal resulted in a different cyclization rate, exothermic reaction, and enthalpy during the  
17 PAN stabilization process.

18

19

## 1 **Experimental**

### 2 **Materials**

3 PAN (average Mw 150,000) and *N, N*-dimethylformamide (DMF) were purchased from  
4 Sigma-Aldrich Korea Co., Ltd. (Republic of Korea). Likewise, copper acetate monohydrate  
5 (CAS No. 6046-93-1), iron acetate (CAS No. 3094-87-9), nickel acetate tetrahydrate (CAS  
6 No. 6018-89-9), and cobalt acetate (CAS No. 71-48-7) were purchased from Sigma-Aldrich  
7 Korea Co., Ltd. These transition metal salts and PAN were first dissolved in DMF separately  
8 as shown in Fig S1 (a) in the supplementary information, and then they were dispersed into  
9 each other to form a 10 wt% of PAN and 0.1 wt% of transition metal salts in DMF (PAN:  
10 metal ion = 99:1) as shown in Fig S1 (b) in the supplementary information.

### 11 **Electrospinning**

12 The electrospinning setup consisted of a positively charged needle nozzle with a high-  
13 voltage DC power supply (Nano NC Co. Ltd., Republic of Korea). The feed rate and applied  
14 voltage were 0.05 mL/h and 10 kV, respectively. The electrospun fibers were deposited onto a  
15 rotating aluminum drum collector at 485 rpm.

### 16 **Thermal oxidative stabilization**

17 PAN stabilization was carried out with the thermal oxidative stabilization. The furnace  
18 was set at four different temperatures: 200 °C, 240 °C, 280 °C, and 320 °C. The fibers were  
19 heat treated for 1 h in air with a temperature increasing rate of 2 °C/min.

### 20 **Characterization**

1 A scanning electron microscope (SEM; JSM-7401F, JEOL, Japan) was used to observe  
2 the withdrawn fibers. FTIR spectrometer (Nicolet iS5, Thermo Fisher Scientific, Waltham,  
3 MA, USA) was used to analyze changes in the chemical composition of the stabilized PAN.  
4 Each sample was scanned 32 times at a resolution of  $4\text{ cm}^{-1}$ . DSC analysis was performed to  
5 measure the heat released during the stabilization process. The conformation of PAN  
6 molecules bonded with the transition metal precursors were visualized using Marvin Sketch  
7 (ChemAxon Ltd., Budapest, Hungary).

## 8 **Results and discussion**

9 The conformation of PAN molecules bonded with various transition metal precursors  
10 were visualized to identify how the transition metal ions affect the stabilization of the  
11 polymer (Fig 1). Owing to the polarity of the acetate from the transition metal precursors, the  
12 opposite sign of the nitrile groups of PAN attracts the carboxyl groups of acetate. As shown in  
13 Fig 1, since the nitrile groups in PAN have high polarity, the  $\text{Co}^{2+}$ ,  $\text{Fe}^{2+}$ , and  $\text{Cu}^{2+}$  ions are  
14 attracted to the negatively charged side (Fig 1). However, because the  $\text{Ni}^{2+}$  ions are  
15 surrounded by negatively charged water molecules, they are prevented from bonding with the  
16 nitrile groups of PAN. Therefore, the positively charged metal ions would affect the redox  
17 properties of the polymer. The microstructure of as-spun PAN and PAN bonded with various  
18 transition metal ions were confirmed by SEM and showed in Fig 1(b-f).

19 The FTIR spectra of the as-spun PAN and PAN bonded with the various transition metal  
20 ions fibers at different stabilization temperatures are presented in Fig 2. The identities of the  
21 peaks are summarized in Table 1. The FTIR spectrum of the as-spun PAN exhibited  
22 characteristic peaks in the range of  $2850\text{--}2940\text{ cm}^{-1}$  for the asymmetric vibration of  $\text{CH}_2$

1 groups ( $\nu_{\text{as(CH}_2\text{)}}$ ), at  $2240\text{ cm}^{-1}$  for the vibration peak of the nitrile groups, and at about  $1650\text{--}$   
2  $1680\text{ cm}^{-1}$  for the vibrational mode of the carbonyl group (C=O highly conjugated from  
3 remaining DMF). The addition of the transition metal precursors to PAN slightly increased  
4 the broad peak from the carboxyl group ( $-\text{COO}^-$ ) in acetate in the range of  $1560\text{--}1590\text{ cm}^{-1}$ .

5 During the thermal oxidative stabilization of PAN, the  $\text{CH}_2$  backbone (at  $2940\text{ cm}^{-1}$ ) lost  
6 hydrogen atoms and the nitrile ( $-\text{C}\equiv\text{N}$ ) peak turned into peaks for the cyclic  $-\text{C}=\text{N}-$  and  $-\text{C}-$   
7  $\text{N}-$  groups. With an increase of the stabilization temperature, the nitrile peak at  $2240\text{ cm}^{-1}$   
8 disappeared and a broad peak of the  $-\text{C}=\text{N}-$ ,  $-\text{N}-\text{H}-$ , and  $\text{C}=\text{C}$  groups appeared at about  $1590$   
9  $\text{cm}^{-1}$ . At the same time, the intensity of the O–H and N–H stretching peaks (at  $3370$  and  $3324$   
10  $\text{cm}^{-1}$ , respectively) gradually appeared with increasing temperatures. The tautomerization of  
11 PAN is generated and initiated by oxygen (in the air), [10, 11] which accepts the lone pair of  
12 electrons from the nitrile groups and dehydrogenates the polymer. The dehydrogenation  
13 process generates free radicals in the PAN molecules, which bind with oxygen to become the  
14 carbonyl groups ( $\nu_{\text{C}=\text{O}}$  peaks at  $1700$  and  $1650\text{ cm}^{-1}$ ). In this way, PAN turns into a ladder-like  
15 structure that makes it non-flammable. Since this reaction occurs at  $200\text{--}300\text{ }^\circ\text{C}$ , we annealed  
16 the PAN molecules with transition metals at the temperatures of  $200\text{ }^\circ\text{C}$ ,  $240\text{ }^\circ\text{C}$ ,  $280\text{ }^\circ\text{C}$ , and  
17  $320\text{ }^\circ\text{C}$  in air.

18 Even though the nitrile groups turned into the cyclic structure in all samples, the  
19 reaction rates were different depending on the assisting transition metal precursor and the  
20 stabilization temperature. The extent of ratio(EOR) for the cyclization reaction was calculated  
21 as follows[46]:

$$22 \quad \text{EOR}(\%) = \frac{I_{1590}}{(I_{2240} + I_{1590})} \times 100$$

1 where  $I_{1590}$  and  $I_{2240}$  are the intensities of the nitrile peaks at 1590 and 2240  $\text{cm}^{-1}$ ,  
2 respectively.

3 As shown in Fig 1, copper acetate monohydrate and cobalt acetate were effective  
4 precursors for initiating the stabilization of PAN over all temperature ranges. According to  
5 the standard hydrogen electrode (SHE), the effectiveness of the ions in initiating the reaction  
6 was predicted to be in the order of  $\text{Cu} > \text{Ni} > \text{Co} > \text{Fe}$  (Table 2). However, according to the  
7 EOR calculation, at 240 °C, the nitrile groups of PAN turned into the cyclic structure in the  
8 order of  $\text{Cu} > \text{Co} > \text{Fe} > \text{Ni}$  (Fig 2f). The stabilization rate of Ni-PAN increased significantly  
9 between 240 °C and 280 °C, which might be due to the evaporation of the water molecules in  
10 the tetrahydrate phase at these temperatures. Moreover, iron acetate hindered the  
11 transformation of the nitrile groups into the cyclic structure.  $\text{Fe}^{2+}$  showed a different behavior  
12 from other metal ions in the PAN stabilization process near 1300  $\text{cm}^{-1}$ , which was related to  
13 oxygen bond in the carboxyl group.

14 To determine the effect of different transition metal ions on the structural evolution and  
15 thermal oxidative stabilization of PAN at 280 °C, FTIR spectral curves of raw PAN and PAN  
16 bonded with the transition metal ions were fitted in the range of 1000–2000  $\text{cm}^{-1}$ . The fitting  
17 curves of the  $\nu_{\text{C=O}}$  peaks (at 1700 and 1650  $\text{cm}^{-1}$ ), the  $\nu_{\text{C=C}} + \nu_{\text{C=N}}$  peak (at 1600  $\text{cm}^{-1}$ ), the  $\nu_{\text{C-N}}$   
18  $\nu_{\text{N-H}}$  peak of amide (at 1525  $\text{cm}^{-1}$ ), the  $\delta_{\text{C-H}}$  peak of  $\text{CH}_2$  (at 1450  $\text{cm}^{-1}$ ), and the  $\nu_{\text{C-CN}}$   
19 peak at 1080  $\text{cm}^{-1}$  are shown in Fig 3.  $\text{Cu}^{2+}$  and  $\text{Co}^{2+}$  in PAN reduced the  $\text{CH}_2$  backbone peak  
20 (at 1450  $\text{cm}^{-1}$ ) and the C–CN peak (at 1080  $\text{cm}^{-1}$ ) more than the other metal ions, indicating a  
21 higher degree of dehydrogenation. In addition, the  $\nu_{\text{C=C}} + \nu_{\text{C=N}}$  peak (at 1590  $\text{cm}^{-1}$ ) was much  
22 higher than the other fitted peaks, suggesting that more cyclization reactions had occurred.  
23 However, the stabilization reaction with Fe-PAN showed a low intensity for the  $\nu_{\text{C=C}} + \nu_{\text{C=N}}$

1 peak and a high intensity for the CH<sub>2</sub> backbone peak. Because of the low cyclization rate, the  
2 peak intensity of  $\delta_{\text{C-H}} + \delta_{\text{N-H}} + \delta_{\text{O-H}}$  in the ring (at 1370 cm<sup>-1</sup>) was also relatively low. In  
3 addition, the intensity ratio of the  $\nu_{\text{C=O}}$  peak at 1700 cm<sup>-1</sup> in Fe-PAN was higher than that of  
4 the other peaks in the other samples. The C=O peak at 1650 cm<sup>-1</sup> represents the conjugated  
5 carbonyl group in the acridone ring, whereas the C=O peak at 1700 cm<sup>-1</sup> is for the  
6 unconjugated carbonyl group in hydronaphthyridine.[10, 14]

7 The peak fitting of FTIR by the Gaussian function in the range of 2150–2300 cm<sup>-1</sup> is  
8 presented in Fig 4. Two new peaks at 2190 and 2210 cm<sup>-1</sup>, identified as  $\beta$ -aminonitrile and  
9 conjugated nitrile, respectively, were associated with the transformation of the nitrile peak at  
10 2240 cm<sup>-1</sup> (Fig 4). These unsaturated nitrile groups are generated by the termination of the  
11 cyclization reaction and dehydrogenation, which can cause structural defects in carbon fiber,  
12 such as chain scissions and point defects.[20] For Fe-PAN, unreacted and unsaturated nitrile  
13 groups remained, indicating insufficient cyclization of the PAN after thermal oxidative  
14 stabilization.

15 As mentioned above, oxidation generates free radicals in the PAN molecules during the  
16 stabilization process, which releases heat. As shown in Fig 5 and Table 3, the DSC  
17 thermogram of raw-PAN in air exhibited a narrow and sharp peak at 296.3 °C. The onset  
18 temperature for raw-PAN was 292.8 °C ( $T_{\text{on}}$ ), and the stabilization process progressed up to  
19 298.9 °C ( $T_{\text{off}}$ ). Here, the free radicals generated a large amount of heat ( $\Delta H = -500$  J/g) in a  
20 temperature change ( $\Delta T$ ) of 6.1 °C. For the PAN molecules that bonded with transition metal  
21 ions, the exothermic peaks occurred at a lower temperature and the thermal oxidative process  
22 released more heat. However, the addition of Fe<sup>2+</sup> and Ni<sup>2+</sup> to PAN did not alleviate the  
23 intense heat generated. In the case of Fe-PAN,  $T_{\text{on}}$  was 265.4 °C and the stabilization process

1 continued to 271.8 °C, with -603 J/g of heat being released during the 6.4 °C ( $\Delta T$ ) increase.  
2 The addition of Fe<sup>2+</sup> ions to PAN also aggravated the heat release rate during the thermal  
3 oxidative stabilization process, as shown in Table 3. In contrast, the addition of Co<sup>2+</sup> or Cu<sup>2+</sup>  
4 to PAN resulted in a longer duration of heat release and a lower T<sub>on</sub> for initiation of the  
5 thermal oxidative process (Fig 5). The DSC peak of Cu-PAN was not only less intense but  
6 was also broader than those of Fe-PAN and Ni-PAN. This indicated that the exothermic  
7 reaction started from a lower temperature and the reaction proceeded without an intensive  
8 exothermic reaction as the temperature increased. The stabilization temperature of Cu-PAN  
9 ranged from 268.3 °C to 276.4 °C with a heat of -598 J/g released. However, the DSC  
10 peak of Co-PAN appeared to be broader, spanning a wide temperature range rather than a  
11 narrow one. As shown in Table 3, the stabilization of Co-PAN was carried out from 249.5 °C  
12 to 269.2 °C ( $\Delta T = 19.7$  °C), with -706 J/g of heat released. We examined the heat release  
13 rates of various thermal oxidative stabilization processes by dividing the amount of heat  
14 generated (during heating of the various PAN samples) by the reaction temperature range  
15 ( $\Delta H/\Delta T$ ). It was determined that the addition of Co<sup>2+</sup> and Cu<sup>2+</sup> to PAN had resulted in the  
16 lowest rates of heat release from the exothermic reaction (Table 3).

17 After the thermal oxidative stabilization process, the stabilized PAN was annealed at  
18 1000 °C with 100 sccm of Ar and 20 sccm of H<sub>2</sub> flowing. TEM images were taken to observe  
19 the effect of added transition metals on the microstructure of the carbon nanofiber, as shown  
20 in Fig 6. No crystalline structure was found in the carbon fibers without any additives, as  
21 shown in Fig 6(a, b), which showed an almost amorphous carbon phase. On the contrary,  
22 carbon fibers containing Fe, Co and Ni have a partially graphitized structure (Fig 6(c-h)).  
23 More specifically, the CNF contain different metals formed by different carbon crystal

1 structures. As an example, the carbon structure of iron in Fig 6(c, d) and Fig S2 in the  
2 Supplementary Information resembled CNT[47, 48]. During the carbonization process, iron  
3 nanoparticles of CNF were spread and merged, while CNT structures were synthesized due to  
4 the catalytic effect of iron nanoparticles. Path traces of the iron nanoparticle changed the  
5 amorphous carbon into a graphitic carbon structure similar to CNT (Fig S2(a)) [49, 50]. In  
6 the case of cobalt shown in Fig 6(e, f) and Fig S3, the existing cobalt nanoparticles caused the  
7 formation of graphitic carbon with a crystalline structure similar to the graphite pockets in  
8 CNF structures [51]. In Fig 6(g, h), with nickel nanoparticles, the graphitic structure was only  
9 found on the nickel surface although the structure was well ordered. Finally, as shown in Fig  
10 6(i, j), no copper nanoparticles were observed in the copper-containing CNFs, revealing the  
11 evaporation of copper during the high-temperature and low-pressure heat treatment. It  
12 showed only an amorphous carbon phase, just like CNF, without additives.

13 Raman spectroscopy was applied to compare the crystallinity depending on the additive  
14 transition metals. As shown in Fig S4, Raman bands from 800 to 2000  $\text{cm}^{-1}$  were fitted with  
15 the Lorentzian (G (1580  $\text{cm}^{-1}$ ), D1 (1350  $\text{cm}^{-1}$ ), D2 (1620  $\text{cm}^{-1}$ ), and D4 (1200  $\text{cm}^{-1}$ )) and  
16 Gaussian (D3 (1510  $\text{cm}^{-1}$ )) line shapes using Origin inbuilt fitting procedures. Consistent  
17 with the TEM data, CNF with iron and cobalt nanoparticles showed higher intensity of G-  
18 band and lower intensity of D3-band than the fibers, indicating the higher content of graphitic  
19  $\text{sp}^2$  phase existed in CNF with iron and cobalt nanoparticles owing to their CNT-like and  
20 graphene-pocket-like graphitic structure observed from TEM, respectively (Fig 6 and Fig S2,  
21 S3). On the contrary, the D3-band presenting around 1510  $\text{cm}^{-1}$  in less crystallized carbon  
22 materials such as amorphous carbon[52, 53] showed higher intensity in raw fibers and in

1 fibers containing nickel and copper additives. This finding is also consistent with the  
2 crystalline structures observed by TEM measurement.

3

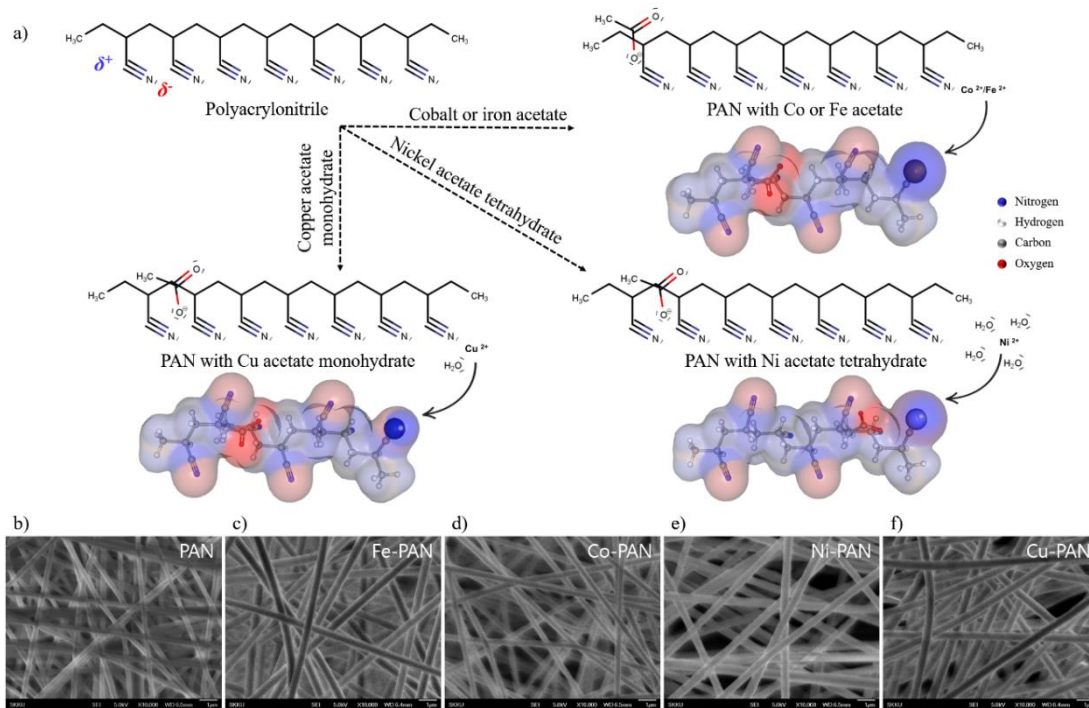
#### 4 **Conclusion**

5 The structural evolution of electrospun PAN nanofibers bonded with different transition  
6 metal precursors was investigated through FTIR and DSC analyses. The cyclization rate and  
7 exothermic reaction of the thermal–oxidative stabilization process were controlled differently  
8 depending on the various transition metal ions used. The addition of the transition metals to  
9 PAN generally decreased the stabilization temperature. With the exception of Fe-PAN, the  
10 transition metals increased the number of cyclization reactions. Notably, the additions of  $\text{Co}^{2+}$   
11 and  $\text{Cu}^{2+}$  alleviated the extensive heat, initiating the thermal oxidative stabilization of PAN at  
12 a lower temperature. Specifically, although the exothermic reaction ( $\Delta H$ ) in Co-PAN  
13 stabilization was increased by approximately 140%, the heat release rate ( $\Delta H/\Delta T$ ) was  
14 alleviated by approximately 44%. The addition of  $\text{Fe}^{2+}$  and  $\text{Co}^{2+}$  also improved the  
15 crystallinity of CNF in 1000 °C heat treatment in a low-pressure Ar and  $\text{H}_2$  environment.

16

1

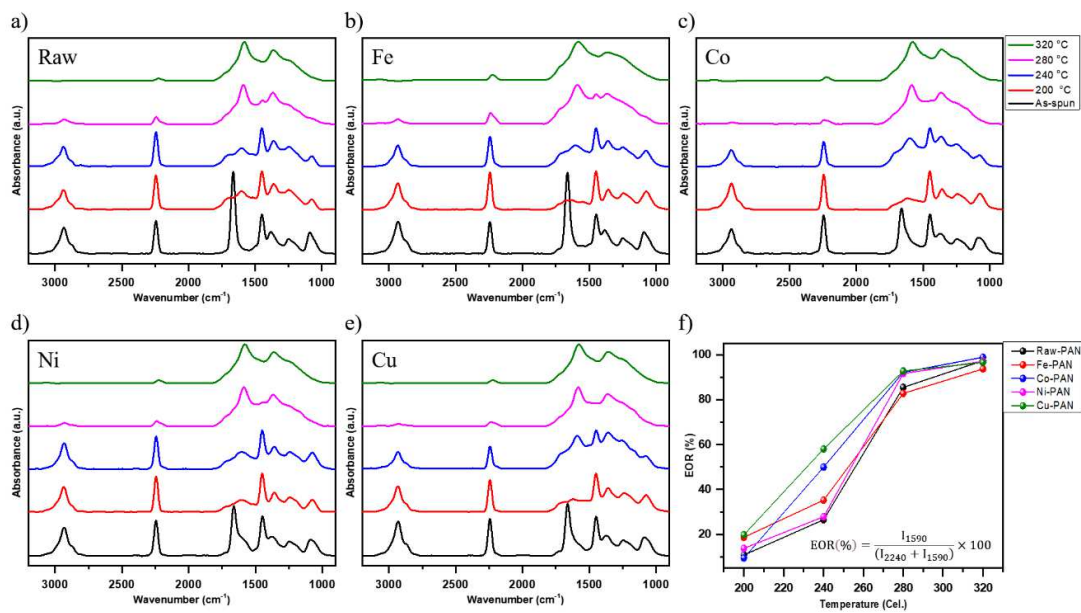
## Figures



2

3 **Fig 1. (a)** Two-dimensional and three-dimensional conformer structures of polyacrylonitrile (PAN) with cobalt  
 4 acetate, iron acetate, copper acetate monohydrate, and nickel acetate tetrahydrate. SEM images of as-spun PAN  
 5 nanofibers (b) without transition metal acetate, (c) with ion acetate, (d) with cobalt acetate, (e) with nickel  
 6 acetate tetrahydrate, and (f) with copper acetate monohydrate.

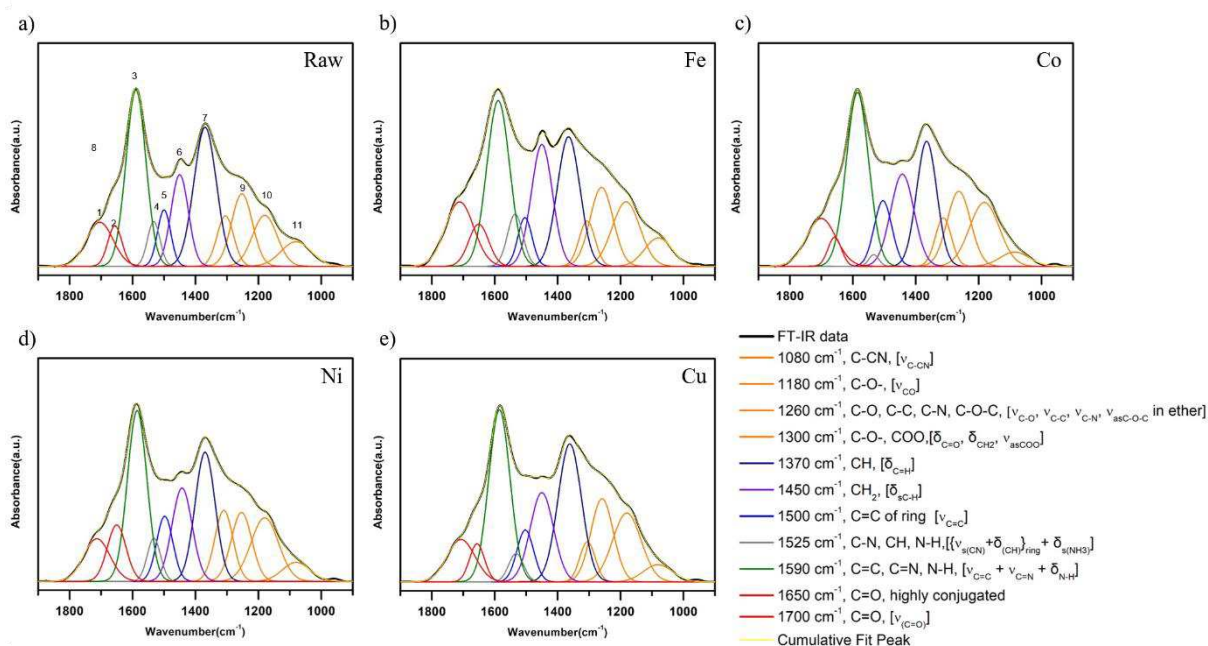
7



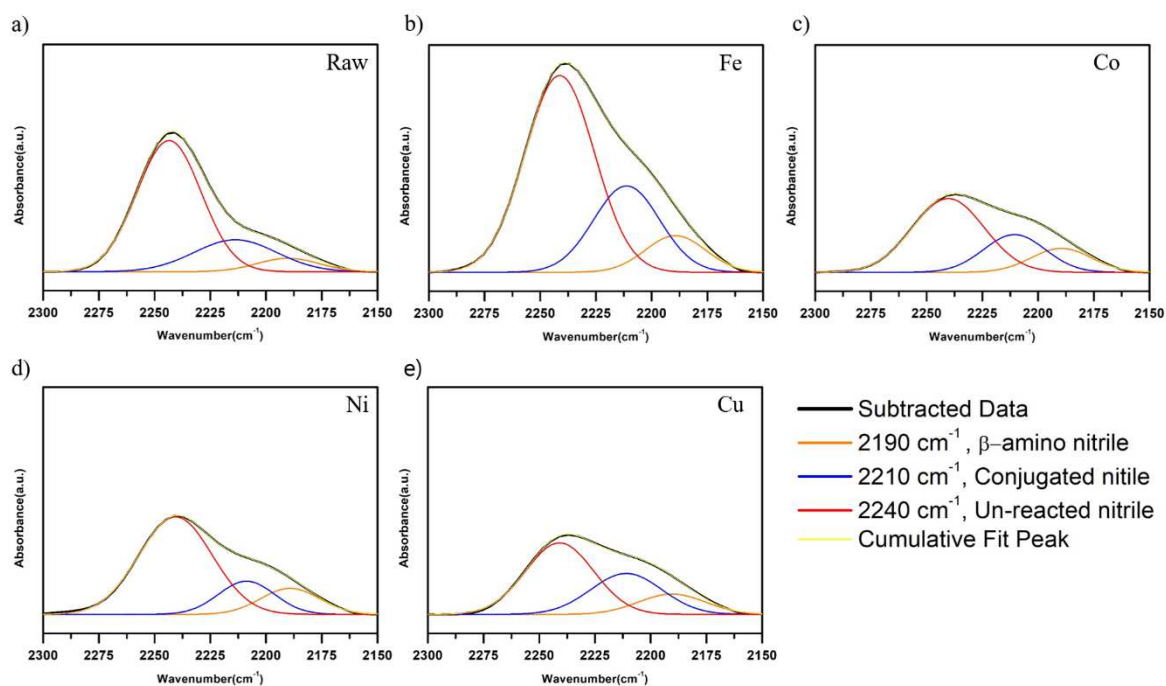
1

2 **Fig 2.** FTIR peaks of polyacrylonitrile (PAN) bonded with transition metal ions according to the various  
 3 stabilization temperatures. (a) Raw PAN; (b) PAN with iron acetate; (c) PAN with cobalt acetate; (d) PAN with  
 4 nickel acetate tetrahydrate; (e) PAN with copper acetate monohydrate; (f) Extent of the cyclization reaction ratio  
 5 (EOR) of PAN with different metal ions according to the stabilization temperature.

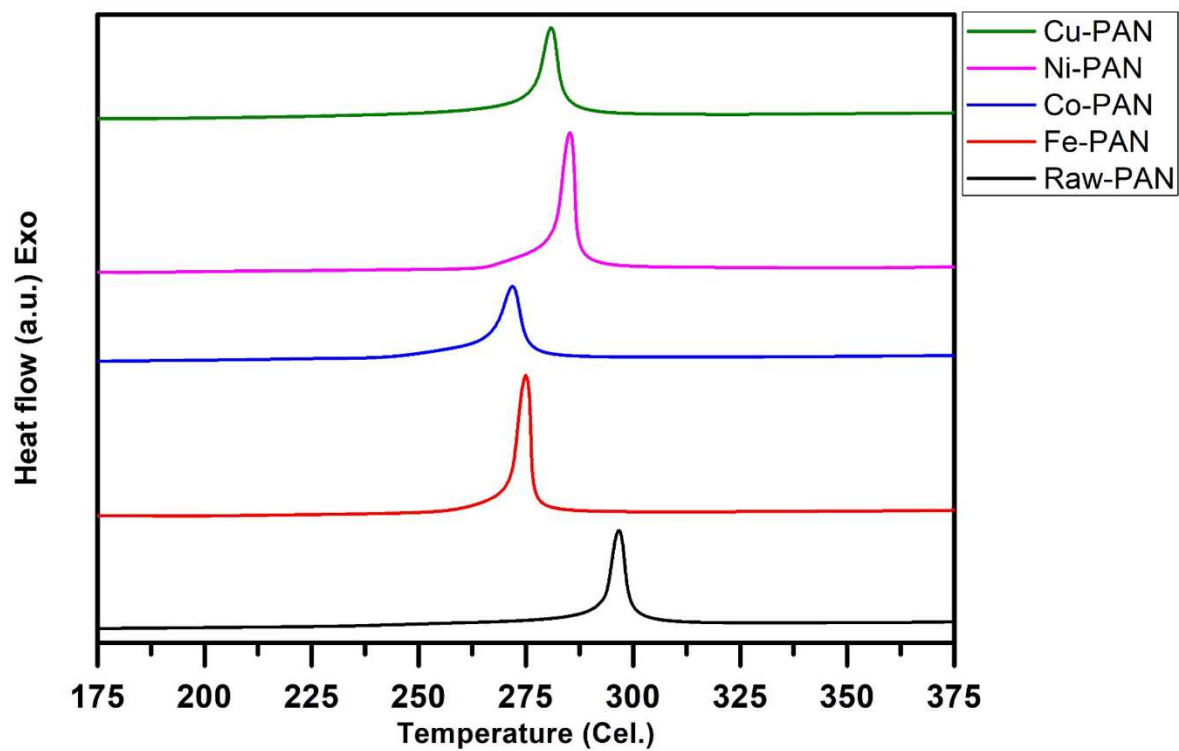
6



1  
2 **Fig 3.** Peak fitting of FTIR peaks by the Gaussian function in the range of 900–2000 cm<sup>-1</sup>. (a) Raw  
3 polyacrylonitrile (PAN) and PAN bonded with (b) Fe<sup>2+</sup>, (c) Co<sup>2+</sup>, (d) Ni<sup>2+</sup>, and (e) Cu<sup>2+</sup>. Thermal oxidative  
4 stabilization was carried out at 280 °C.



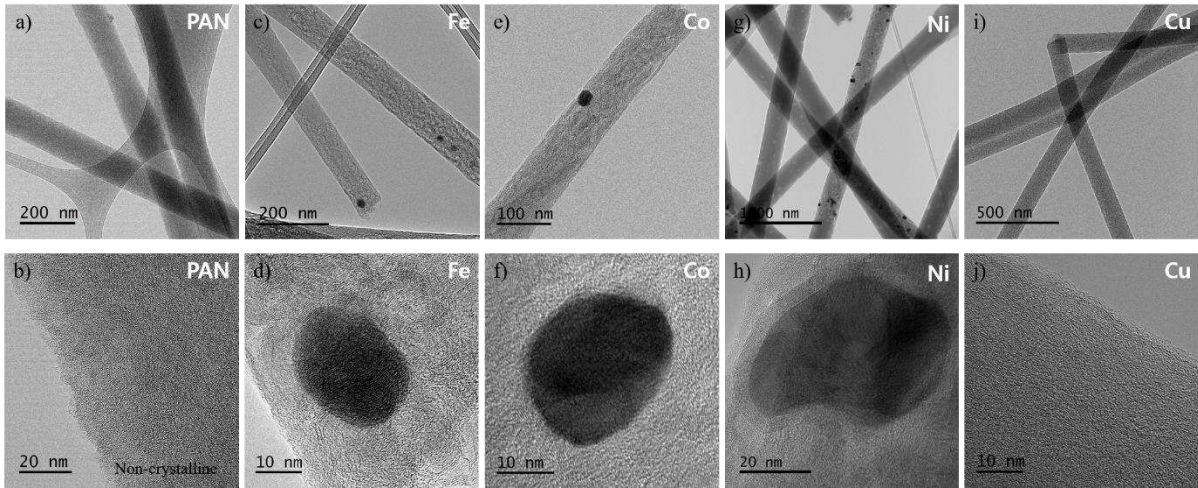
5  
6 **Fig 4.** Peak fitting of FTIR peaks by the Gaussian function in the range of 2150–2300 cm<sup>-1</sup>. (a) Raw  
7 polyacrylonitrile (PAN) and PAN bonded with (b) Fe<sup>2+</sup>, (c) Co<sup>2+</sup>, (d) Ni<sup>2+</sup>, and (e) Cu<sup>2+</sup>. Thermal oxidative  
8 stabilization was carried out at 280 °C.



1

2 **Fig 5.** Differential scanning calorimetry (DSC) thermograms of polyacrylonitrile (PAN) bonded with various  
3 transition metal ions in the air.

4



1  
2  
3  
4  
5

**Fig 6.** TEM images of CNF (a, b) without any additive, with (c, d) iron, (d, f) cobalt, (g, h) nickel nanoparticles, and with (i-j) copper acetate monohydrate as additive.

| As spun PAN                    |                    |   |  |                      | After stabilization            |                      |   |  |                      |
|--------------------------------|--------------------|---|--|----------------------|--------------------------------|----------------------|---|--|----------------------|
| Wavenumber (cm <sup>-1</sup> ) | Group              | Vibration type                              | Assignment   | Ref.                 | Wavenumber (cm <sup>-1</sup> ) | Group                | Vibration type  | Assignment   | Ref.                 |
| 1070–1080                      | C-CN               | $\nu_{C-CN}$                                |  | [10, 14]             | 1070–1080                      | C-CN                 | $\nu_{C-CN}$  |  | [10, 14]             |
| 1080–1100                      | CH                 |   | Aliphatic ethers, alcohols   | [34]                 | 1160–1190                      | C-O-                 | $\nu_{CO}$  | $\alpha$ , $\beta$ -unsaturated esters and carboxylic acids                | [10, 14]             |
| 1190–1200                      | C=O                |   | C-O group in $\alpha$ , $\beta$ -unsaturated esters and carboxylic acids | [14]                 | 1230–1260                      | C-O, C-C, C-N, C-O-C | $\nu_{C-O}, \nu_{C-C}, \nu_{C-N}$<br>$\nu_{asC-O-C}$ in ether |  | [10, 14]             |
| 1245–1255                      | C-O                | $\nu_{CO}$                                  |  | [14]                 | 1290–1330                      | C-O-, COO            | $\delta_{C-O}, \delta_{CH_2}, \nu_{asCOO}$                    |  | [14, 35, 36]         |
| 1310–1320                      | C-O-               | $\delta_{C-O}, \delta_{CH_2}$ at C-6        |  | [14, 35]             | 1360–1370                      | C-H + N-H + OH       | $\delta_{C-H} + \delta_{N-H} + \delta_{O-H}$                  | C-H, N-H, O-H in ring  | [14, 35]             |
| 1340–1365                      | CH                 | $\delta_{C-H}$                              |  | [14]                 | 1420–1450                      | C-H                  | $\delta_{sC-H}$   | in CH <sub>2</sub>   | [10, 14, 34, 36, 37] |
| 1375–1395                      | C-H, N-H, O-H      | $\delta_{C-H} + \delta_{N-H} + \delta_{OH}$ |  | [10, 38]             | 1490–1510                      | C=C                  | $\nu_{C=C}$   | Of ring, Tyr-O <sup>-</sup> or Trp   | [10, 39, 40]         |
| 1450                           | CH <sub>2</sub>    | $\delta_{CH}$ flat                          | CH <sub>2</sub> bending (scissoring)                                     | [10, 37]             | 1520–1540                      | C-N, CH, N-H         | $[\nu_{s(CN)} + \delta_{(CH)}]_{ring} + \delta_{s(NH_3)}$     | Tyr-OH, amide  | [10, 41, 42]         |
| 1560–1590                      | -COO <sup>-</sup>  |   | Carboxyl group in salt from -COO <sup>-</sup>                            | [34]                 | 1590–1620                      | C=C, C=N, N-H        | $\nu_{C=C} + \nu_{C=N} + \delta_{N-H}$                        | Cyclic structure originated from cyclization and dehydrogenation reactions | [10, 43]             |
| 1620                           | RCOO-              | $\nu_{asC-O}$                               | Carboxylate anion  | [14]                 | 1640–1660                      | C=O                  |   | Highly conjugated, acridone ring   | [34, 41]             |
| 1650–1680                      | C=O, C=C, C=N      | $\nu_{C=O}, \nu_{C=C} + \nu_{C=N}$          | C=O highly conjugated (from DMF)   | [34] [10]            | 1700–1730                      | C=O                  | $\nu_{s(C=O)}$  | Ketone, aldehyde, and -COOH  | [10, 34, 39]         |
| 1710                           | RCOOR'             | Stretching                                  | Carbonyl group in $\alpha, \beta$ -unsaturated esters                    | [14]                 | 2170–2190                      |                      |   | $\beta$ -amino   | [14, 20][21][44]     |
| 1730                           | RCOOH              | Stretching                                  | Carbonyl group in $\alpha, \beta$ -unsaturated acids                     | [14]                 | 2200–2220                      |                      |   | Conjugated nitrile   | [14, 20][21][44]     |
| 2240–2243                      | C≡N                |   | Unreacted nitrile  | [14, 21, 38, 44, 45] | 2240–2243                      | C≡N                  |   | Unreacted nitrile  | [14, 21, 38, 44, 45] |
| 2850–2870                      | -O-CH <sub>3</sub> |   |  | [14, 35]             |                                |                      |   |  |                      |
| 2930–2940                      | -C-H               | Asymmetric $\nu_{CH_2}$                     |  | [14, 35]             |                                |                      |   |  |                      |

1 **Table 1. Interpretation of the FTIR absorbance peaks of polyacrylonitrile (PAN) and PAN bonded with different transition metal ions during the**  
2 **thermal-oxidative stabilization process.**

3  $\nu$ : Stretching vibration;  $\delta$ : Bending vibration; as: asymmetric; s: symmetric; DMF: *N, N*-dimethylformamide

**Table 2. Standard hydrogen electrode (SHE).**

| <b>Oxidant</b>  |          | <b>Reductant</b>        | <b>E<sup>0</sup> (V)</b> |
|---|----------|-------------------------|--------------------------|
| <b>Fe<sup>2+</sup> + 2e<sup>-</sup></b>                   | <b>↔</b> | <b>Fe(s)</b>            | <b>-0.44</b>             |
| <b>Co<sup>2+</sup> + 2e<sup>-</sup></b>                   | <b>↔</b> | <b>Co(s)</b>            | <b>-0.28</b>             |
| <b>Ni<sup>2+</sup> + 2e<sup>-</sup></b>                   | <b>↔</b> | <b>Ni(s)</b>            | <b>-0.25</b>             |
| <b>2H<sup>+</sup> + 2e<sup>-</sup></b>                    | <b>↔</b> | <b>H<sub>2</sub>(g)</b> | <b>0.0000</b>            |
| <b>Cu<sup>2+</sup> + 2e<sup>-</sup></b>                   | <b>↔</b> | <b>Cu(s)</b>            | <b>+0.337</b>            |
| <b>Cu<sup>+</sup> + e<sup>-</sup></b>                     | <b>↔</b> | <b>Cu(s)</b>            | <b>+0.520</b>            |
| <b>O<sub>2</sub>(g) + 4H<sup>+</sup> + 4e<sup>-</sup></b> | <b>↔</b> | <b>2H<sub>2</sub>O</b>  | <b>+1.229</b>            |

**Table 3. Differential scanning calorimetry (DSC) data of the heat released during the stabilization of raw polyacrylonitrile (PAN) and PAN bonded with transition metal ions from 195 °C to 325 °C upon heating at 10 °C/min in air atmosphere.**

| Sample  | DSC in air           |                       |         |                     |          |  |
|---------|----------------------|-----------------------|---------|---------------------|----------|--|
|         | T <sub>on</sub> (°C) | T <sub>off</sub> (°C) | ΔT (°C) | T <sub>p</sub> (°C) | ΔH (J/g) | ΔH/ΔT (J·g <sup>-1</sup> ·°C <sup>-1</sup> ) |
| Raw-PAN | 292.8                | 298.9                 | 6.1     | 296.3               | -500     | 81.97  |
| Fe-PAN  | 265.4                | 271.8                 | 6.4     | 269.6               | -603     | 94.21  |
| Co-PAN  | 249.5                | 269.2                 | 19.7    | 262                 | -706     | 35.84  |
| Ni-PAN  | 272.6                | 279.2                 | 6.6     | 276.8               | -620     | 93.94  |
| Cu-PAN  | 268.3                | 276.4                 | 8.1     | 273.1               | -598     | 73.83  |

- T<sub>on</sub>: temperature at the onset of stabilization.
- T<sub>off</sub>: temperature at the end of stabilization.
- ΔT: temperature change
- T<sub>p</sub>: peak temperature of stabilization
- ΔH: enthalpy change

**Acknowledgments**

This work was supported by a grant from the Korea Evaluation Institute of Industrial Technology (KEIT) funded by the Ministry of Trade, Industry & Energy (MOTIE) [NO. 20012341].

**Declarations****Conflicts of interest**

The authors have no conflicts of interest to declare that are relevant to the content of this article.

**Code availability**

Not applicable.

## References

1. H. Morgan, Carbon Fibers and Their Composites, (CRC Press, Boca Raton, 2005).
2. J. B. Donnet, T. K. Wang, J.C. Peng, S. Rebouillat, Carbon Fibers, 3<sup>rd</sup> edn. (Marcel Dekker, New York, 1998).
3. E. Fitzer, Carbon Fibers and Their composites, (Springer, New York, 1985).
4. D.D. Edie, Carbon 364 345-362 (1998).
5. E. Fitzer, carbon 275 25 (1989).
6. E. Frank, F. Hermanutz, M.R. Buchmeiser, Macromolecular Materials and Engineering 2976 493-501 (2012).
7. O.-K. Park, S. Lee, H.-I. Joh, J.K. Kim, P.-H. Kang, J.H. Lee, B.-C. Ku, Polymer 5311 2168-2174 (2012).
8. S. CHAND, JOURNAL OF MATERIALS SCIENCE 35 10 (2000).
9. R.V. Ghorpade, D.W. Cho, S.C. Hong, Carbon 121 502-511 (2017).
10. N.U. Nguyen-Thai, S.C. Hong, Macromolecules 4615 5882-5889 (2013).
11. Z. Fu, Y. Gui, S. Liu, Z. Wang, B. Liu, C. Cao, H. Zhang, Journal of Applied Polymer Science 13119 (2014).
12. Y. Xue, J. Liu, J. Liang, Polymer Degradation and Stability 981 219-229 (2013).
13. S.-P. Rwei, T.-F. Way, Y.-S. Hsu, Polymer Degradation and Stability 9810 2072-2080 (2013).
14. E.V. Loginova, I.V. Mikheev, D.S. Volkov, M.A. Proskurnin, Anal. Methods 82 371-380 (2016).
15. J. Hao, Y. Liu, C. Lu, Polymer Degradation and Stability 147 89-96 (2018).
16. D.U. Park, N.K. Han, J.H. Ryu, W.H. Park, Y.G. Jeong, Fibers and Polymers 1910 2007-2015 (2018).
17. J.D. Moskowitz, W. Jacobs, A. Tucker, M. Astrove, B. Harmon, Polymer Degradation and Stability 178 109198 (2020).
18. H. Liu, S. Zhang, J. Yang, M. Ji, J. Yu, M. Wang, X. Chai, B. Yang, C. Zhu, J. Xu, Polymers 117 1150 (2019).
19. S.K.C.a.R.C.P. G. AYREY, Journal of polymer Science: Polymer Chemistry Edition 20 10 (1982).
20. X. Qin, Y. Lu, H. Xiao, Y. Song, Materials Letters 76 162-164 (2012).

21. X. Li, A. Qin, X. Zhao, D. Liu, H. Wang, C. He, *Phys Chem Chem Phys* 1734 21856-65 (2015).
22. H.G. Chae, M.L. Minus, A. Rasheed, S. Kumar, *Polymer* 4813 3781-3789 (2007).
23. M. Mohammadi, A. Rezaei, A. Khazaei, S. Xuwei, Z. Huajun, *ACS applied materials & interfaces* 1136 33194-33206 (2019).
24. P. Hayati, S. Suárez-García, A. Gutierrez, E. Şahin, D.R. Molina, A. Morsali, A.R. Rezvani, *Ultrasonics sonochemistry* 42 310-319 (2018).
25. A. Ansari, S. Vahedi, O. Tavakoli, M. Khoobi, M.A. Faramarzi, *Applied Organometallic Chemistry* 331 e4634 (2019).
26. T. Mortezaazadeh, E. Gholibegloo, N. Riyahi Alam, S. Haghgoo, A. Musa, M. Khoobi, *Journal of Biomedical Physics & Engineering* 101 25 (2020).
27. S. Okazoe, Y. Yasaka, M. Kudo, H. Maeno, Y. Murakami, Y. Kimura, *Chemical Communications* 5456 7834-7837 (2018).
28. Q. Bai, F.C. Shen, S.L. Li, J. Liu, L.Z. Dong, Z.M. Wang, Y.Q. Lan, *Small Methods* 212 1800049 (2018).
29. L. Xu, L. Zhang, B. Cheng, J. Yu, *Carbon* 152 652-660 (2019).
30. B. Zhang, Z.-L. Xu, Y.-B. He, S. Abouali, M.A. Garakani, E.K. Heidari, F. Kang, J.-K. Kim, *Nano Energy* 4 88-96 (2014).
31. B. Bajaj, H.-I. Joh, S.M. Jo, J.H. Park, K.B. Yi, S. Lee, *Applied Surface Science* 429 253-257 (2018).
32. H. Tang, W. Chen, J. Wang, T. Dugger, L. Cruz, D. Kisailus, *Small* 1411 1703459 (2018).
33. M.A.A.M. Abdah, N.H.N. Azman, S. Kulandaivalu, Y. Sulaiman, *Materials & Design* 186 108199 (2020).
34. Y. Chen, C. Zou, M. Mastalerz, S. Hu, C. Gasaway, X. Tao, *Int J Mol Sci* 1612 30223-50 (2015).
35. D. Koutsianitis, C. Mitani, K. Giagli, D. Tsalagkas, K. Halasz, O. Kolonics, C. Gallis, L. Csoka, *Ultrason Sonochem* 23 148-55 (2015).
36. C.-B.W. Hung-Kuan Lin, Hui-Chi Chiu, and Shu-Hua Chien, *Catalysis Letters* 86 6 (2003).
37. B. Minčeva-Šukarova, B. Mangovska, G. Bogojeva-Gaceva, V.M. Petruševski, *Croatica Chemica Acta* 10.5562/cca1888 63-70 (2012).
38. J. Zhao, J. Zhang, T. Zhou, X. Liu, Q. Yuan, A. Zhang, *RSC Adv.* 66 4397-4409 (2016).
39. A. Barth, *Progress in Biophysics & Molecular Biology* 74 33 (2000).
40. X. Colom, F. Carrillo, F. Nogués, P. Garriga, *Polymer Degradation and Stability* 803 543-549 (2003).

41. I.A. Mudunkotuwa, V.H. Grassian, *Langmuir* 3029 8751-60 (2014).
42. M. Wolpert, P. Hellwig, *Spectrochim Acta A Mol Biomol Spectrosc* 644 987-1001 (2006).
43. H.K.a.K. Tashiro, *Polymer Journal* 294 5 (1997).
44. Y. Liu, *Stabilization and carbonization studies of polyacrylonitrile/carbon nanotube composite fibers*, The School of Polymer, Textile and Fiber Engineering, Georgia Institute of Technology, 2010.
45. M.A. Phadke, D.A. Musale, S.S. Kulkarni, S.K. Karode, *Journal of Polymer Science Part B: Polymer Physics* 4315 2061-2073 (2005).
46. M.A.W.a.S.K.M. Y. Zhu, *JOURNAL OF MATERIALS SCIENCE* 31 7 (1996).
47. B.A. Newcomb, L.A. Giannuzzi, K.M. Lyons, P.V. Gulgunje, K. Gupta, Y. Liu, M. Kamath, K. McDonald, J. Moon, B. Feng, *Carbon* 93 502-514 (2015).
48. K. Zhao, Z.-Y. Liu, B.-L. Xiao, D.-R. Ni, Z.-Y. Ma, *Acta Metallurgica Sinica (English Letters)* 312 134-142 (2018).
49. B.J. Mapleback, T.J. Simons, Y. Shekibi, K. Ghorbani, A.N. Rider, *Electrochimica Acta* 331 135233 (2020).
50. H. Wang, X. Li, F. Meng, G. Wang, D. Zhang, *Chemical Engineering Journal* 392 123798 (2020).
51. T. Lehnert, M.K. Kinyanjui, A. Ladenburger, D. Rommel, K. Wörle, F. Börrnert, K. Leopold, U. Kaiser, *ACS nano* 118 7967-7973 (2017).
52. D.G. Henry, I. Jarvis, G. Gillmore, M. Stephenson, *Earth-Science Reviews* 198 102936 (2019).
53. M. Pawlyta, J.-N. Rouzaud, S. Duber, *Carbon* 84 479-490 (2015).

# Figures

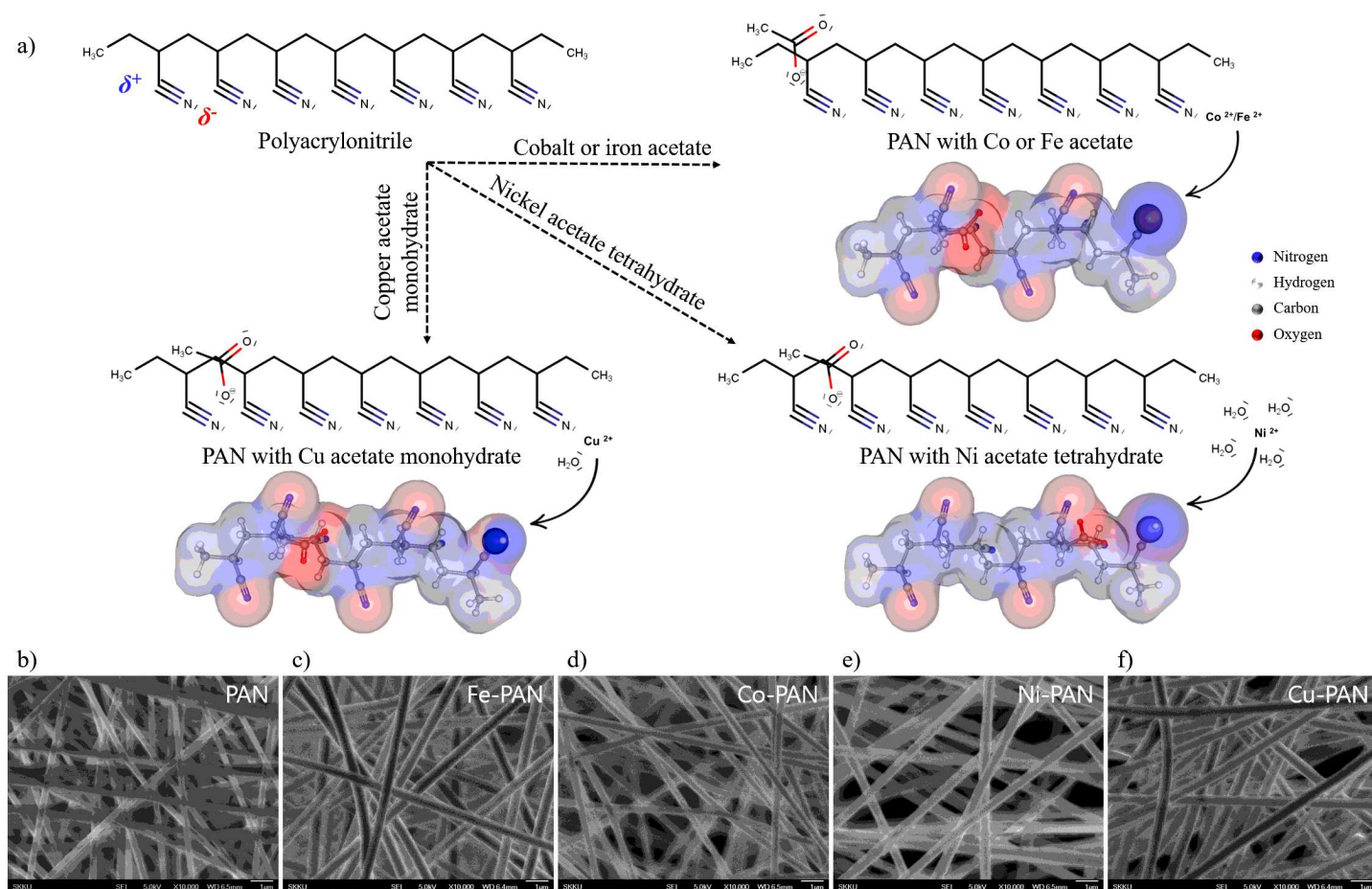


**Figure 1**

(a) Two-dimensional and three-dimensional conformer structures of polyacrylonitrile (PAN) with cobalt acetate, iron acetate, copper acetate monohydrate, and nickel acetate tetrahydrate. SEM images of as-spun PAN nanofibers (b) without transition metal acetate, (c) with iron acetate, (d) with cobalt acetate, (e) with nickel acetate tetrahydrate, and (f) with copper acetate monohydrate.

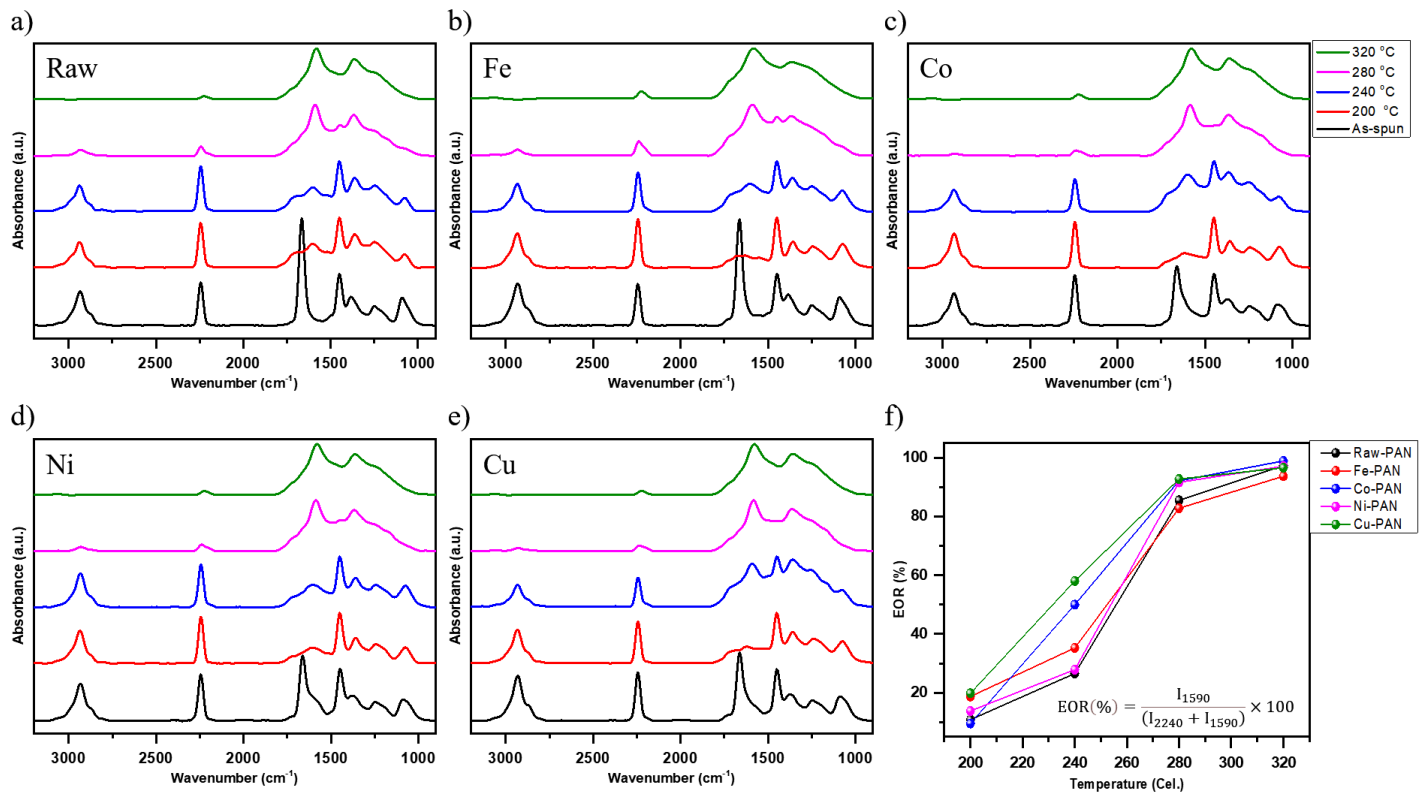


**Figure 2**

FTIR peaks of polyacrylonitrile (PAN) bonded with transition metal ions according to the various stabilization temperatures. (a) Raw PAN; (b) PAN with iron acetate; (c) PAN with cobalt acetate; (d) PAN with nickel acetate tetrahydrate, (e) PAN with copper acetate monohydrate; (f) Extent of the cyclization reaction ratio (ECM) of PAN with different metal ions according to the stabilization temperature.

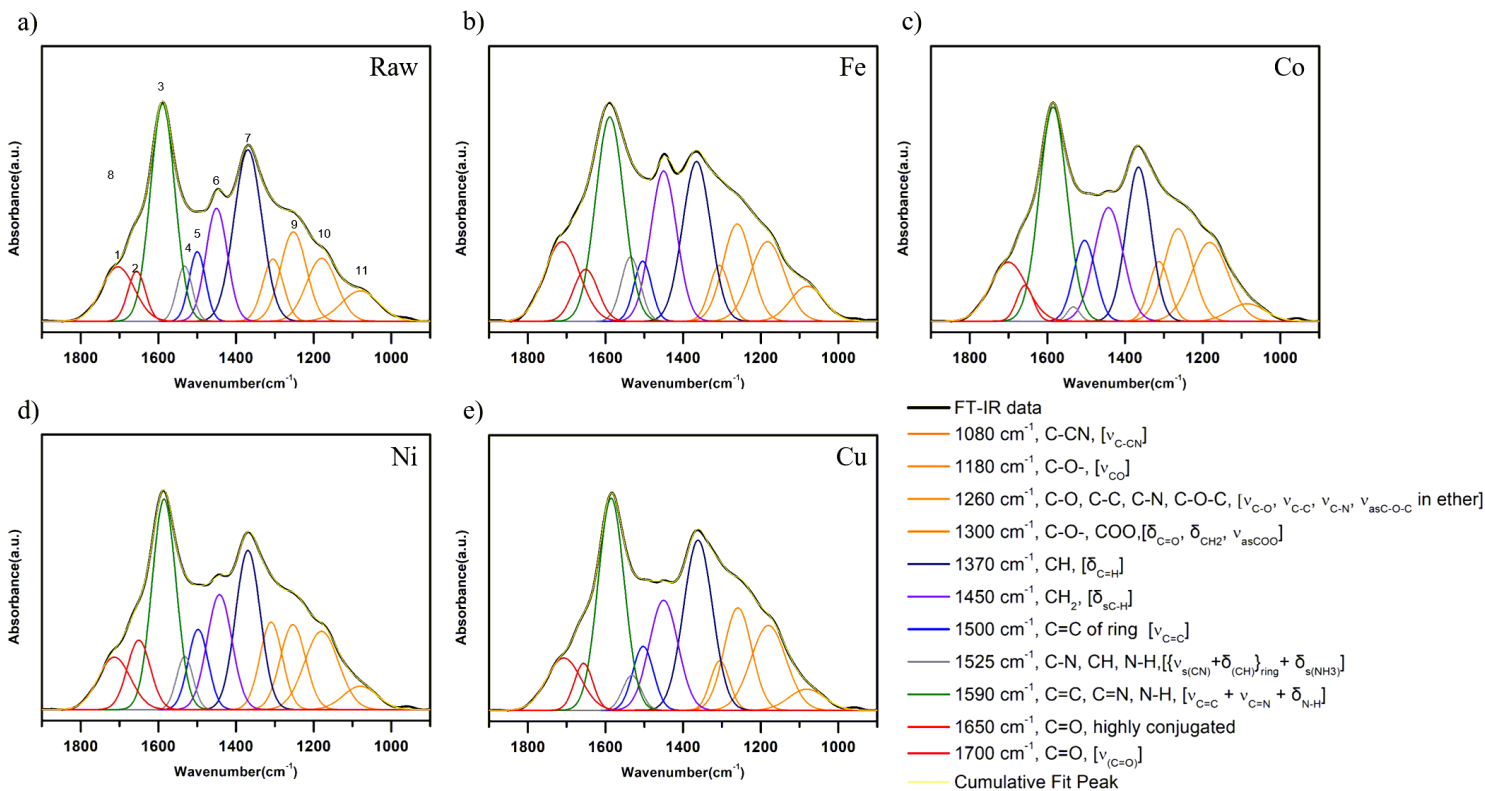


**Figure 3**

Peak fitting of FUR peaks by the Gaussian function in the range of 900-2000 cm<sup>-1</sup>. (a) Raw polyacrylonitrile (PAN) and PAN bonded with (lb) Fe<sup>2+</sup>, (c) Co<sup>2+</sup>, (d) Ni<sup>2+</sup>, and (e) Cu<sup>2+</sup>. Thermal oxidative stabilization was carried out at 280 °C.

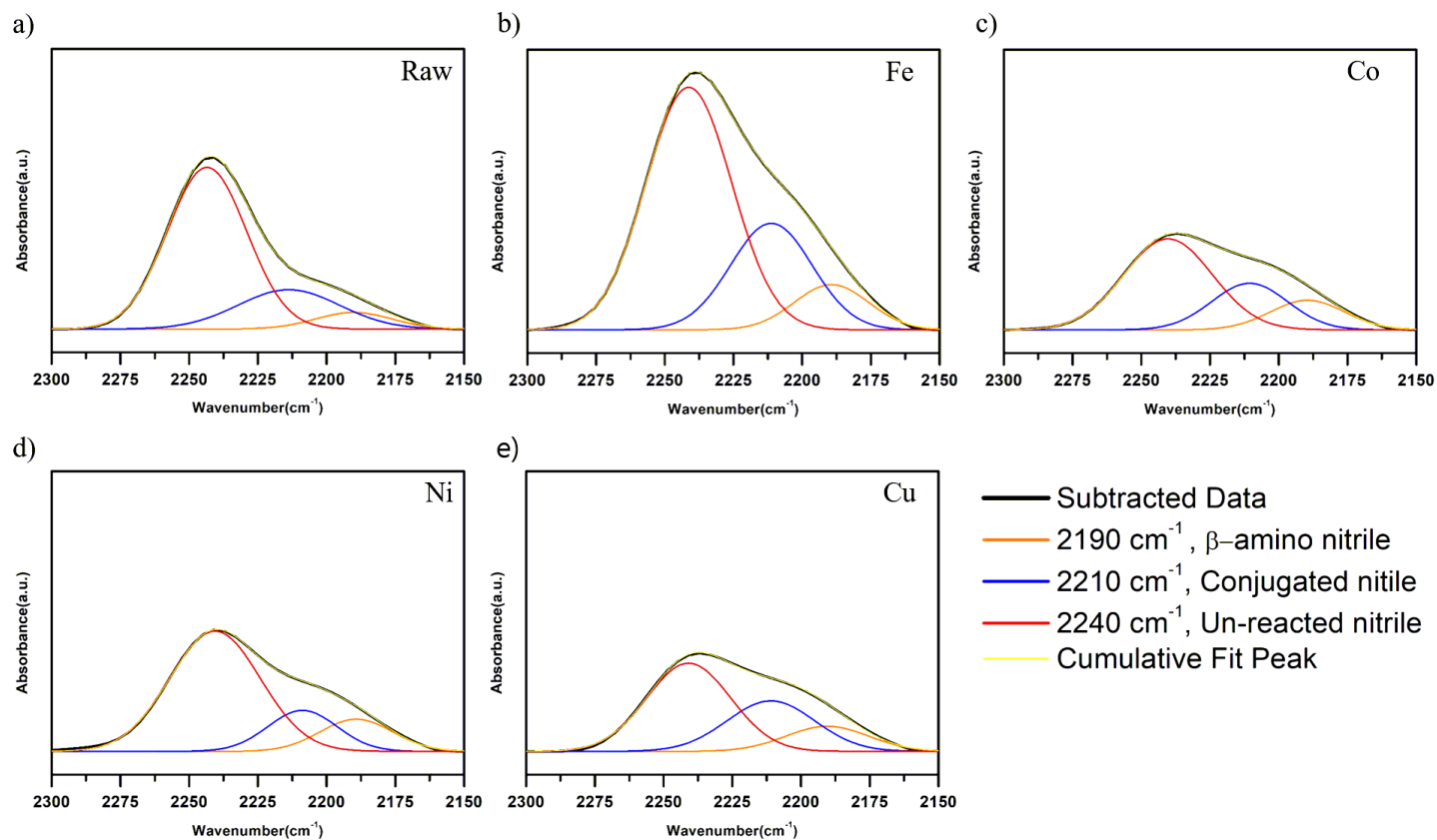


**Figure 4**

Peak fitting of MIR peaks by the Gaussian function in the range of 2150-2300  $\text{cm}^{-1}$ . (a) Raw polyacrylonitrile (PAN) and PAN bonded with (b) Fe, (c) (d) Ni, and (e) Cu. Thermal oxidative stabilization was carried out at 280  $^{\circ}\text{C}$ .

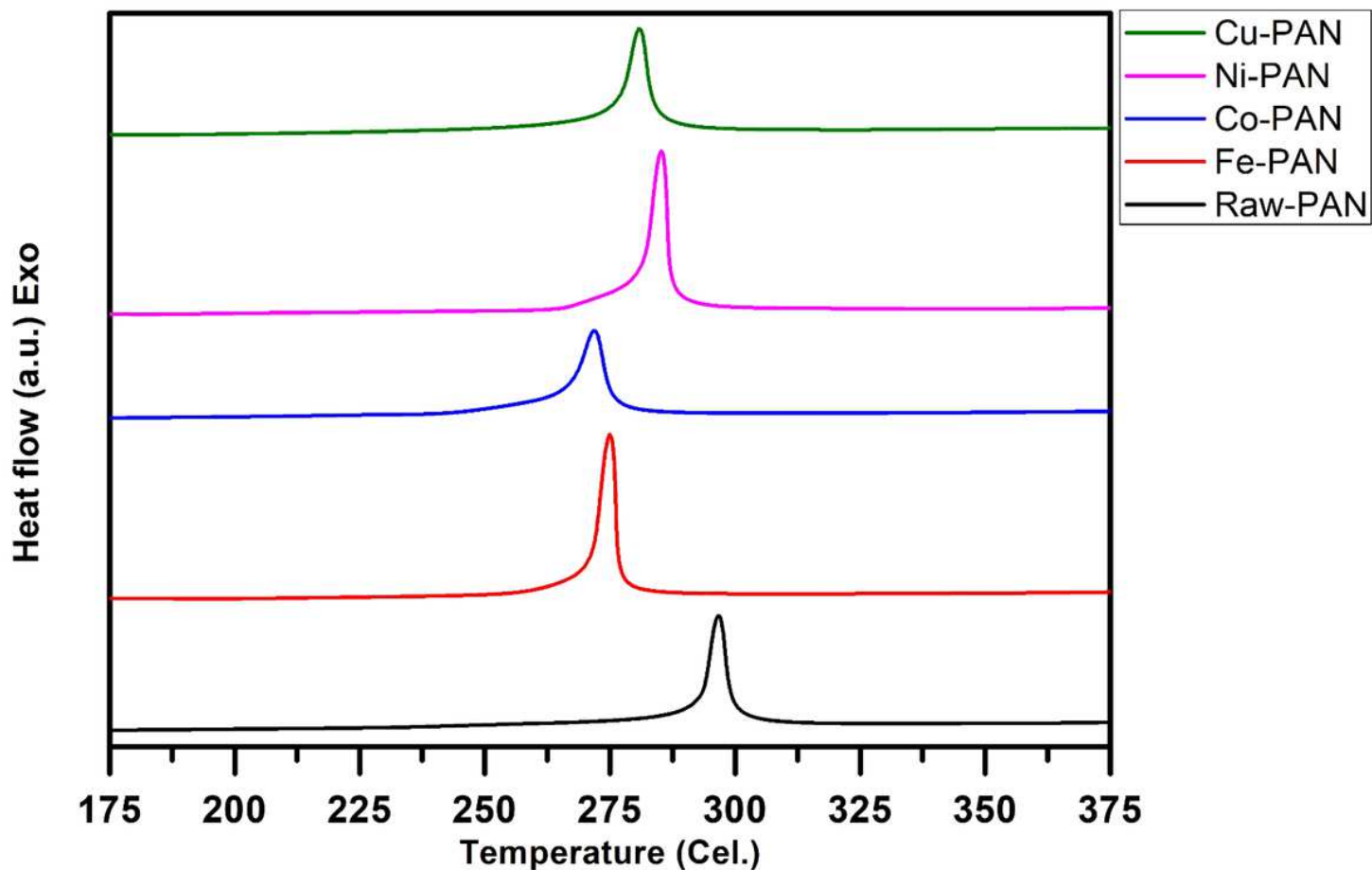
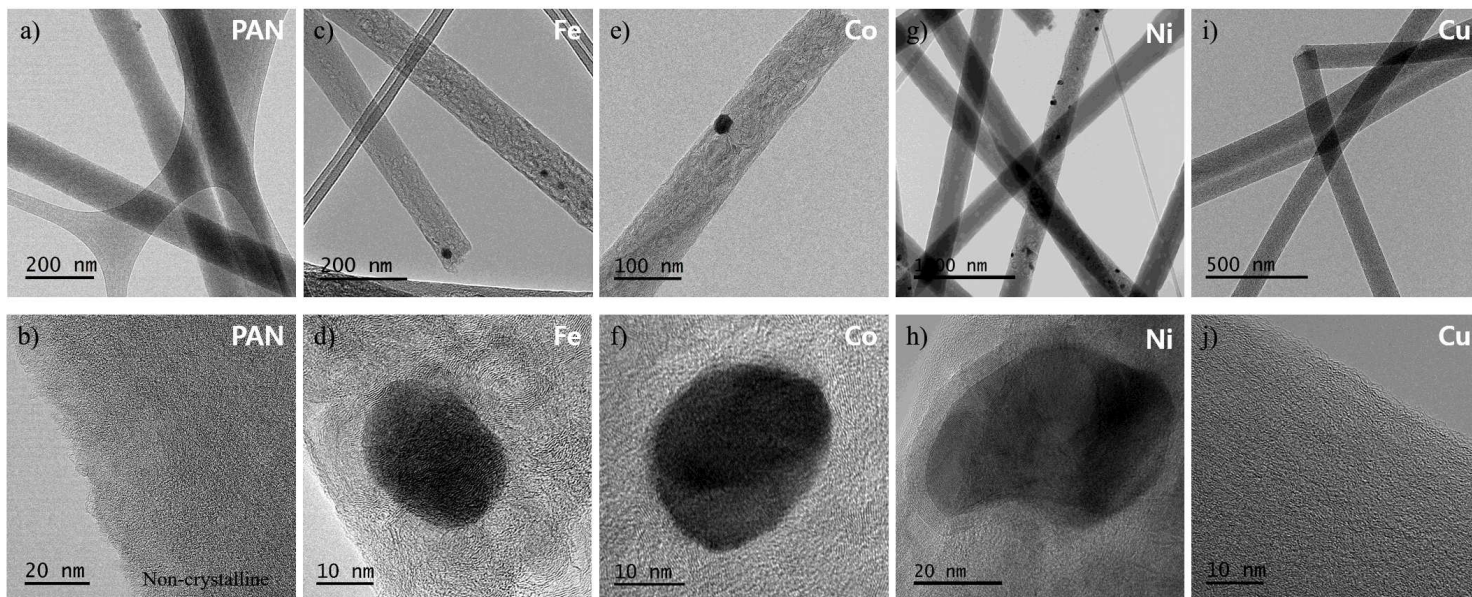


Figure 5

Differential scanning calorimetry (DSC) thermograms of polyacrylonitrile (PAN) bonded with various transition metal ions in the air.



## Figure 6

TEM images of CNF (a, b) without any additive, with (r, d) iron, (d, l) cobalt, (g, h) nickel nanoparticles, and with (i-j) copper acetate monohydrate as additive.

## Supplementary Files

This is a list of supplementary files associated with this preprint. Click to download.

- [SupplementaryInformation.docx](#)
- [table1.pdf](#)
- [table3.pdf](#)
- [table2.pdf](#)